Acta Mech 225, 609–623 (2014)
DOI 10.1007/s00707-013-0976-1

M. Hemmatnezhad · G. H. Rahimi · R. Ansari

On the free vibrations of grid-stiffened composite cylindrical shells

Received: 27 March 2013 / Revised: 20 July 2013 / Published online: 20 September 2013

Abstract A unified analytical approach is applied for investigating the vibrational behavior of grid-stiffened composite cylindrical shells considering the flexural behavior of the ribs. A smeared method is employed to superimpose the stiffness contribution of the stiffeners with those of the shell in order to obtain the equivalent stiffness parameters of the whole panel. The stiffeners are modeled as a beam and considered to support shear loads and bending moments in addition to the axial loads. Therefore, the corresponding stiffness terms are taken into consideration while obtaining the stiffness matrices due to the stiffeners. Theoretical formulations are based on first-order shear deformation shell theory, which includes the effects of transverse shear deformation and rotary inertia. The modal forms are assumed to have the axial dependency in the form of Fourier series whose derivatives are legitimized using Stokes' transformation. In order to validate the obtained results, a 3-D finite element model is also built using ABAQUS CAE software. Results obtained from two types of analyses are compared with each other, and good agreement has been achieved. Furthermore, the influence of variations in the shell thickness and changes of the boundary conditions on the shell frequencies is studied. The results obtained are novel and can be used as a benchmark for further studies.

1 Introduction

The vibration analysis of cylindrical shells (e.g., frequencies, mode shapes, and modal forces) is a well-established branch of research in structural dynamics. Cylindrical shells due to their high strength as well as light weight have gained many applications in civil, mechanical, and aerospace engineering (e.g., launch vehicles, reentry vehicles, aircraft fuselages, spacecrafts, etc.) in particular. The large number of publications which has been expanded rapidly in the past decades testifies to this fact. An excellent collection of research in this area was carried out by Leissa [1]. There are also some good reviews on vibration of composite shells using experimental [2,3] and analytical methods [4–10], and numerical techniques [11–15]. Based upon the first-order shear deformation theory, Ansari and Darvizeh [16] presented a general analytical approach for investigating the vibrational behavior of functionally graded cylindrical shells. Recently, Hemmatnezhad et al. [17] investigated the vibrational behavior of composite cylindrical shells using the same analytical approach as in [16] and based on different shell theories.

Grid-stiffened cylinders are cylinders with stiffening structures either on the inner, outer, or both sides of the shell. These stiffeners significantly increase the load resistance of a cylinder without much increase in weight. The optimum kind of stiffener configuration is chosen based on the type of application, the loading condition,

M. Hemmatnezhad · G. H. Rahimi (✉)
Department of Mechanical Engineering, Tarbiat Modares University, P.O. Box 14115-143, Tehran, Iran
E-mail: rahimi_gh@modares.ac.ir

R. Ansari
Department of Mechanical Engineering, University of Guilan, P.O. Box 3756, Rasht, Iran

cost, and other factors. The promising future of stiffened cylinders has led to a wide range of research work [18–25].

The number of publications dealing with the mechanical behavior of composite cylinders with cross stiffeners is scarce, and most of the related researches are associated with stiffened cylinders with longitudinal and circumferential stiffeners. Kidane and his associates [26,27] derived the buckling loads of a generally cross and horizontal grid-stiffened composite cylinder by developing a smeared method for determination of the equivalent stiffness parameters of a grid-stiffened composite cylindrical shell. Afterward, Yazdani [28] and Yazdani and Rahimi [29] performed experimental investigations on the buckling behavior of composite cylindrical shells with cross stiffeners. They also studied the effects of the number of helical ribs and changes in grid types on the buckling load of these structures [30,31]. Recently, Rahimi and his co-associates studied the effect of the stiffener cross-section profile on the buckling strength of composite stiffened cylindrical shells by implementing the finite element method [32].

The vibration analysis of grid-stiffened cylindrical shells has not been seen in the literature to the best of the authors' knowledge. In the present work, a calculation of the overall response of composite cylindrical shells with cross stiffeners is presented using an exact analytical approach and based upon first-order shear deformation theory. A smeared method is employed to superimpose the stiffness contribution of the stiffeners with those of the shell in order to obtain the equivalent stiffness parameters of the whole panel [26,27].

In the smeared method proposed in the previous studies [26,27], it is assumed that the transverse modulus of the unidirectional stiffeners is much lower than the longitudinal modulus. Therefore, the stiffeners are assumed to be two-force members supporting axial loads only, and the capability of supporting shear loads and bending moments is not considered for them. The vibrational analysis of the grid composite cylinders considering the flexural behavior of the ribs has not been carried out before. Since shear loads are effective forces in composite structures and bending moments are more important in the buckling and vibrational behaviors, ignoring theses effects may give analytical results with higher errors.

The present work deals with free vibration analysis of composite stiffened cylindrical shells under arbitrary boundary conditions. The aim is to find a precise and effective mathematical model capable of predicting the vibrational characteristics of stiffened cylinders to avoid performing multiple experiments. A smeared method is employed to superimpose the stiffness contribution of the stiffeners with those of the shell in order to obtain the equivalent stiffness parameters of the whole panel. In addition to the axial load, the stiffeners are also assumed to support shear loads and bending moments. Then, a general analytical approach based on the first-order shear deformation theory [16] is used to find the natural frequencies of vibration. The modal forms are assumed to have the axial dependency in the form of Fourier series whose derivatives are legitimized using Stokes' transformation [10,17]. Furthermore, the influence of variations in the shell thickness and changes of the boundary conditions on the shell frequencies is studied. The results obtained are novel and can be used as a benchmark for further studies.

2 Equivalent stiffnesses

Consider a cylindrical shell reinforced with a lozenge-type stiffener structure as shown in Fig. 1. First of all, it is required to determine the equivalent stiffness parameters of the overall structure in order to calculate the vibration frequencies of a composite cylinder with inner stiffening structure.

The analytical tool employed for this, so-called the smeared stiffener approach, uses a mathematical model to smear the stiffeners into an equivalent laminate and determine the equivalent stiffness of the laminate. The procedure is similar to that used in [26,27] but based on the following refined assumptions:

1. The shear stresses in the cross stiffeners are not to be ignored.
2. The cross-section dimensions of the stiffeners are very small compared to the length.
3. A uniform stress distribution is assumed across the cross-sectional area of the stiffeners.
4. The stiffeners are modeled as a beam and considered to support shear loads and bending moments further to the axial loads.
5. The load on the stiffener/shell is transferred through shear forces between the stiffeners and shell.
6. In the loading condition, the cross sections of the stiffeners do not go under torsion.

2.1 Force analysis

Based on the laminated plate theory, the strains on the interface of the stiffener and the shell are given by

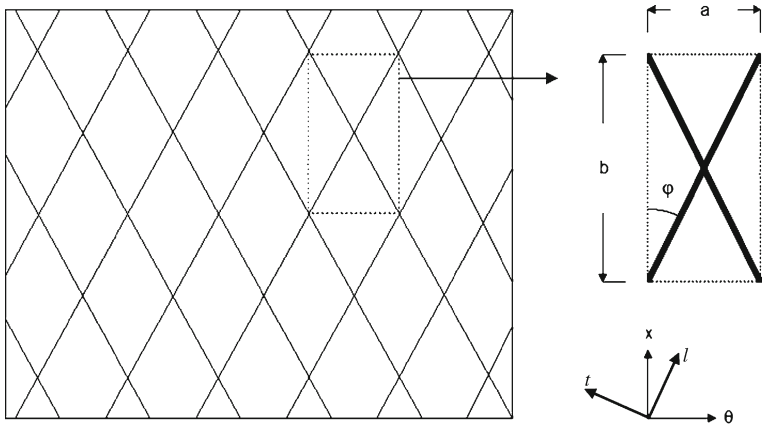

Fig. 1 Unit cell and coordinate system for a stiffened cylindrical shell

$$\begin{aligned}
\varepsilon_{xx} &= \varepsilon^0_{xx} + \left(\frac{t}{2}\right)\kappa_x,\\
\varepsilon_{\theta\theta} &= \varepsilon^0_{\theta\theta} + \left(\frac{t}{2}\right)\kappa_\theta,\\
\varepsilon_{x\theta} &= \varepsilon^0_{x\theta} + \left(\frac{t}{2}\right)\kappa_{x\theta},\\
\varepsilon_{\theta z} &= \varepsilon^0_{\theta z},\\
\varepsilon_{zx} &= \varepsilon^0_{zx},
\end{aligned} \tag{1}$$

which can be considered as the strain components in the cross-section of the stiffeners. In the above relation, t is the shell thickness and $\varepsilon^0_{xx}, \varepsilon^0_{\theta\theta}, \varepsilon^0_{x\theta}, \varepsilon^0_{\theta z}, \varepsilon^0_{zx}, \kappa_x, \kappa_\theta, \kappa_{x\theta}$ describe the mid-plane strains and curvatures of the shell. To resolve these strain components along the stiffener direction (l) and normal to it (t), one can use the following transformation matrix:

$$\begin{bmatrix} \varepsilon_l \\ \varepsilon_t \\ \varepsilon_{tz} \\ \varepsilon_{zl} \\ \varepsilon_{lt} \end{bmatrix} = \begin{bmatrix} c^2 & s^2 & 0 & 0 & cs \\ s^2 & c^2 & 0 & 0 & -cs \\ 0 & 0 & c & s & 0 \\ 0 & 0 & -s & c & 0 \\ -2cs & -2cs & 0 & 0 & c^2 - s^2 \end{bmatrix} \begin{bmatrix} \varepsilon_{xx} \\ \varepsilon_{\theta\theta} \\ \varepsilon_{\theta z} \\ \varepsilon_{zx} \\ \varepsilon_{x\theta} \end{bmatrix}, \tag{2}$$

where $c = \cos\phi$, $s = \sin\phi$, and ϕ are the stiffener orientation angle. Figure 2 shows the forces on the unit cell of the stiffener structure.

Substituting the appropriate angle into Eq. (2) and applying assumptions (2) and (3), one can reach the axial and shear forces in the stiffener direction as

$$\begin{aligned}
F_{l1} &= A_l E_l \varepsilon_{l1} = A_l E_l \left(c^2\varepsilon_{xx} + s^2\varepsilon_{\theta\theta} + cs\varepsilon_{x\theta}\right),\\
F_{l2} &= A_l E_l \varepsilon_{l2} = A_l E_l \left(c^2\varepsilon_{xx} + s^2\varepsilon_{\theta\theta} - cs\varepsilon_{x\theta}\right),\\
F_{lt1} &= A_l G_{lt} \varepsilon_{lt1} = A_l G_{lt} \left(-2cs\varepsilon_{xx} - 2cs\varepsilon_{\theta\theta} + (c^2 - s^2)\varepsilon_{x\theta}\right),\\
F_{lt2} &= A_l G_{lt} \varepsilon_{lt2} = A_l G_{lt} \left(2cs\varepsilon_{xx} + 2cs\varepsilon_{\theta\theta} + \left(c^2 - s^2\right)\varepsilon_{x\theta}\right),
\end{aligned} \tag{3}$$

where E_l and G_{lt} are the longitudinal and shear modulus of the stiffeners, respectively. Resolving the axial and shear forces in the x and θ directions and then summing up the axial and circumferential forces applying on the sides of the unit cell, one arrives at

$$\begin{aligned}
F_x &= (F_{l1} + F_{l2})\, c + (F_{lt1} + F_{lt2})\, s,\\
F_\theta &= (F_{l1} + F_{l2})\, s - (F_{lt1} + F_{lt2})\, c.
\end{aligned} \tag{4}$$

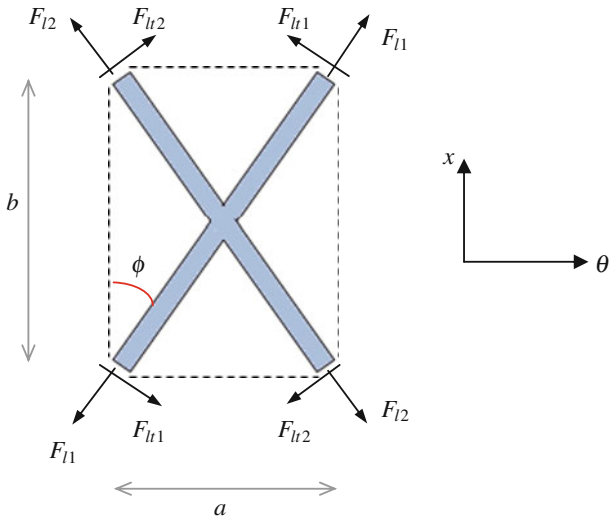

Fig. 2 Force distribution on the unit cell

The shear force is obtained by summing the forces along any sides of the unit cell as

$$F_{x\theta} = (F_{l1} - F_{l2})\, c + (F_{lt1} - F_{lt2})\, s. \tag{5}$$

Substitution for strain components from Eq. (1) into Eq. (3), using Eqs. (4) and (5) and dividing the force expressions by the corresponding edge width of the unit cell, gives the forces per unit length as

$$\begin{aligned}
N_x^{\mathrm{st}} &= \frac{2A_l E_l c^3}{a}\varepsilon_{xx}^0 + \frac{2A_l E_l s^2 c}{a}\varepsilon_{\theta\theta}^0 + \frac{2A_l G_{lt}(c^2-s^2)s}{a}\varepsilon_{x\theta}^0 + \frac{A_l E_l c^3 t}{a}\kappa_x \\
&\quad + \frac{A_l E_l s^2 ct}{a}\kappa_\theta + \frac{A_l G_{lt}(c^2-s^2)\mathrm{st}}{a}\kappa_{x\theta}, \\
N_\theta^{\mathrm{st}} &= \frac{2A_l E_l c^2 s}{b}\varepsilon_{xx}^0 + \frac{2A_l E_l s^3}{b}\varepsilon_{\theta\theta}^0 + \frac{2A_l G_{lt}(c^2-s^2)c}{b}\varepsilon_{x\theta}^0 + \frac{A_l E_l c^2 \mathrm{st}}{b}\kappa_x \\
&\quad + \frac{A_l E_l s^3 t}{b}\kappa_\theta + \frac{A_l G_{lt}(c^2-s^2)ct}{b}\kappa_{x\theta}, \\
N_{x\theta}^{\mathrm{st}} &= -\frac{4A_l G_{lt} cs^2}{b}\varepsilon_{xx}^0 - \frac{4A_l G_{lt} cs^2}{b}\varepsilon_{\theta\theta}^0 + \frac{2A_l E_l c^2 s}{b}\varepsilon_{x\theta}^0 - \frac{2A_l G_{lt} cs^2 t}{b}\kappa_x \\
&\quad - \frac{2A_l G_{lt} cs^2 t}{b}\kappa_\theta + \frac{A_l E_l c^2 \mathrm{st}}{b}\kappa_{x\theta},
\end{aligned} \tag{6}$$

where the superscript 'st' stands for the stiffeners. These forces should be transferred to the mid-plane of the shell. While transferring, bending moments are produced due to the distance among the points of application of the reaction forces in the stiffeners and the mid-plane of the shell. These bending moments will be obtained in the following section.

2.2 Moment analysis

As pointed before, the reaction moments due to the stiffeners are produced by the shear forces on the interface of the stiffener and the shell. The moment caused by these forces on the mid-plane of the shell equals the forces multiplied by one half the shell thickness. Figure 3 shows the moment free body diagram of a unit cell. M_1 and M_2 are the moments resulting from forces F_1 and F_2, respectively. Following the same manner as above for the force analysis on a unit cell, the resultant moments on the horizontal and vertical sides can be obtained as

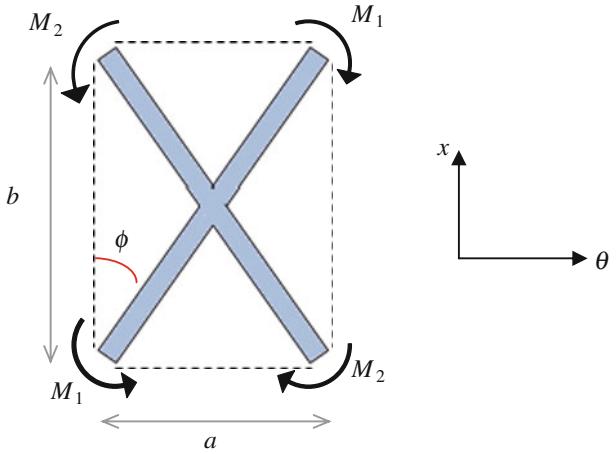

Fig. 3 Moments due to the stiffeners

$$
\begin{aligned}
M_x^{\mathrm{st}} &= \frac{A_l E_l c^3 t}{a}\varepsilon_{xx}^0 + \frac{A_l E_l s^2 ct}{a}\varepsilon_{\theta\theta}^0 + \frac{A_l G_{lt}(c^2-s^2)\mathrm{st}}{a}\varepsilon_{x\theta}^0 + \frac{A_l E_l c^3 t^2}{2a}\kappa_x \\
&\quad + \frac{A_l E_l s^2 ct^2}{2a}\kappa_\theta + \frac{A_l G_{lt}(c^2-s^2)\mathrm{st}^2}{2a}\kappa_{x\theta}, \\
M_\theta^{\mathrm{st}} &= \frac{A_l E_l c^2 \mathrm{st}}{b}\varepsilon_{xx}^0 + \frac{A_l E_l s^3 t}{b}\varepsilon_{\theta\theta}^0 + \frac{A_l G_{lt}(c^2-s^2)ct}{b}\varepsilon_{x\theta}^0 + \frac{A_l E_l c^2 \mathrm{st}^2}{2b}\kappa_x \\
&\quad + \frac{A_l E_l s^3 t^2}{2b}\kappa_\theta + \frac{A_l G_{lt}(c^2-s^2)ct^2}{2b}\kappa_{x\theta}, \\
M_{x\theta}^{\mathrm{st}} &= -\frac{2A_l G_{lt} cs^2 t}{b}\varepsilon_{xx}^0 - \frac{2A_l G_{lt} cs^2 t}{b}\varepsilon_{\theta\theta}^0 + \frac{A_l E_l c^2 \mathrm{st}}{b}\varepsilon_{x\theta}^0 - \frac{A_l G_{lt} cs^2 t^2}{2b}\kappa_x \\
&\quad - \frac{A_l G_{lt} cs^2 t^2}{2b}\kappa_\theta + \frac{A_l E_l c^2 \mathrm{st}^2}{2b}\kappa_{x\theta}.
\end{aligned}
\tag{7}
$$

2.3 Shear force analysis

In a plane with normal vector z, the strain component ε_{lz} can be written as

$$
\varepsilon_{lz} = s\varepsilon_{\theta z} + c\varepsilon_{zx}. \tag{8}
$$

The shear forces resulting from shear strains are given as

$$
\begin{aligned}
F_{lz1} &= A_l G_{lz}(s\varepsilon_{\theta z}^0 + c\varepsilon_{zx}^0), \\
F_{lz2} &= A_l G_{lz}(-s\varepsilon_{\theta z}^0 + c\varepsilon_{zx}^0).
\end{aligned}
\tag{9}
$$

Resolving these forces in the x and θ directions and then summing up the forces on the upper and lower sides of the unit cell, we arrive at

$$
\begin{aligned}
q_x^{\mathrm{st}} &= (F_{lz1} + F_{lz2})\, c, \\
q_\theta^{\mathrm{st}} &= (F_{lz1} + F_{lz2})\, s,
\end{aligned}
\tag{10}
$$

which in terms of Eq. (9) can be rewritten as

$$
q_x^{\mathrm{st}} = 2A_l G_{lz} c^2 \varepsilon_{zx}^0,\ q_\theta^{\mathrm{st}} = 2A_l G_{lz} cs\varepsilon_{zx}^0. \tag{11}
$$

The resultant shear forces per unit length can be obtained by dividing the above forces by the corresponding length as

$$Q_x^{\mathrm{st}} = \frac{2A_l G_{lz} c^2}{a}\varepsilon_{zx}^0, \quad Q_\theta^{\mathrm{st}} = \frac{2A_l G_{lz} cs}{b}\varepsilon_{zx}^0, \tag{12}$$

which can be arranged in matrix form as

$$\begin{bmatrix} Q_x^{\mathrm{st}} \\ Q_\theta^{\mathrm{st}} \end{bmatrix} = \begin{bmatrix} \frac{2A_l G_{lz} c^2}{a} & 0 \\ \frac{2A_l G_{lz} cs}{b} & 0 \end{bmatrix} \begin{bmatrix} \varepsilon_{zx}^0 \\ \varepsilon_{z\theta}^0 \end{bmatrix}. \tag{13}$$

2.4 Stiffness matrices

Equations (6) and (7) denote the force and moment contributions of the stiffener, respectively. These equations are summarized in matrix form below:

$$\begin{bmatrix} N_x^{\mathrm{st}} \\ N_\theta^{\mathrm{st}} \\ N_{x\theta}^{\mathrm{st}} \\ M_x^{\mathrm{st}} \\ M_\theta^{\mathrm{st}} \\ M_{x\theta}^{\mathrm{st}} \end{bmatrix} = \begin{bmatrix} \frac{2A_l E_l c^3}{a} & \frac{2A_l E_l s^2 c}{a} & \frac{2A_l G_{lt}(c^2-s^2)s}{a} & \frac{A_l E_l c^3 t}{a} & \frac{A_l E_l s^2 ct}{a} & \frac{A_l G_{lt}(c^2-s^2)\mathrm{st}}{a} \\ \frac{2A_l E_l c^2 s}{b} & \frac{2A_l E_l s^3}{b} & \frac{2A_l G_{lt}(c^2-s^2)c}{b} & \frac{A_l E_l c^2 \mathrm{st}}{b} & \frac{A_l E_l s^3 t}{b} & \frac{A_l G_{lt}(c^2-s^2)ct}{b} \\ -\frac{4A_l G_{lt} cs^2}{b} & -\frac{4A_l G_{lt} cs^2}{b} & \frac{2A_l E_l c^2 s}{b} & -\frac{2A_l G_{lt} cs^2 t}{b} & -\frac{2A_l G_{lt} cs^2 t}{b} & \frac{A_l E_l c^2 \mathrm{st}}{b} \\ \frac{A_l E_l c^3 t}{a} & \frac{A_l E_l s^2 ct}{a} & \frac{A_l G_{lt}(c^2-s^2)\mathrm{st}}{a} & \frac{A_l E_l c^3 t^2}{2a} & \frac{A_l E_l s^2 ct^2}{2a} & \frac{A_l G_{lt}(c^2-s^2)\mathrm{st}^2}{2a} \\ \frac{A_l E_l c^2 \mathrm{st}}{b} & \frac{A_l E_l s^3 t}{b} & \frac{A_l G_{lt}(c^2-s^2)ct}{b} & \frac{A_l E_l c^2 \mathrm{st}^2}{2b} & \frac{A_l E_l s^3 t^2}{2b} & \frac{A_l G_{lt}(c^2-s^2)ct^2}{2b} \\ -\frac{2A_l G_{lt} cs^2 t}{b} & -\frac{2A_l G_{lt} cs^2 t}{b} & \frac{A_l E_l c^2 \mathrm{st}}{b} & -\frac{A_l G_{lt} cs^2 t^2}{2b} & -\frac{A_l G_{lt} cs^2 t^2}{2b} & \frac{A_l E_l c^2 \mathrm{st}^2}{2b} \end{bmatrix} \begin{bmatrix} \varepsilon_{xx}^0 \\ \varepsilon_{\theta\theta}^0 \\ \varepsilon_{x\theta}^0 \\ \kappa_x \\ \kappa_\theta \\ \kappa_{x\theta} \end{bmatrix}. \tag{14}$$

Also, the shear forces due to the stiffeners are given by Eq. (13). The resultant force and moments due to the shell in terms of the strain components of the mid-plane surface of the shell can be written as

$$\begin{bmatrix} N_x^{\mathrm{sh}} \\ N_\theta^{\mathrm{sh}} \\ N_{x\theta}^{\mathrm{sh}} \\ M_x^{\mathrm{sh}} \\ M_\theta^{\mathrm{sh}} \\ M_{x\theta}^{\mathrm{sh}} \\ Q_x^{\mathrm{sh}} \\ Q_\theta^{\mathrm{sh}} \end{bmatrix} = \begin{bmatrix} A_{11} & A_{12} & 0 & B_{11} & B_{12} & 0 & 0 & 0 \\ A_{12} & A_{22} & 0 & B_{12} & B_{22} & 0 & 0 & 0 \\ 0 & 0 & A_{66} & 0 & 0 & B_{66} & 0 & 0 \\ B_{11} & B_{12} & 0 & D_{11} & D_{12} & 0 & 0 & 0 \\ B_{12} & B_{22} & 0 & D_{12} & D_{22} & 0 & 0 & 0 \\ 0 & 0 & B_{66} & 0 & 0 & D_{66} & 0 & 0 \\ 0 & 0 & 0 & 0 & 0 & 0 & A'_{44} & 0 \\ 0 & 0 & 0 & 0 & 0 & 0 & 0 & A'_{55} \end{bmatrix} \begin{bmatrix} \varepsilon_{xx}^0 \\ \varepsilon_{\theta\theta}^0 \\ \varepsilon_{x\theta}^0 \\ \kappa_x \\ \kappa_\theta \\ \kappa_{x\theta} \\ \varepsilon_{xz}^0 \\ \varepsilon_{\theta z}^0 \end{bmatrix}, \tag{15}$$

in which $A'_{44} = KA_{44}$, $A'_{55} = KA_{55}$, K is known as a correction factor and 'sh' superscript stands for the shell. Moreover, the stiffnesses of the shell are given as

$$\left(A_{ij}, B_{ij}, D_{ij}\right) = \int_{-\frac{t}{2}}^{\frac{t}{2}} Q_{ij}(1, z, z^2)\mathrm{d}z, \tag{16}$$

where Q_{ij} are the plane stress-reduced stiffnesses, and t is the uniform thickness of the shell with the reference middle surface. The total force and moment on the panel are the superposition of the forces and moments due to the stiffeners and the shell according to their volume fractions as

$$\begin{bmatrix} N \\ M \end{bmatrix} = \begin{bmatrix} V_{\mathrm{st}} N^{\mathrm{st}} + V_{\mathrm{sh}} N^{\mathrm{sh}} \\ V_{\mathrm{st}} M^{\mathrm{st}} + V_{\mathrm{sh}} M^{\mathrm{sh}} \end{bmatrix}. \tag{17}$$

Fig. 4 A 3-D model of the grid-stiffened cylinder used in the present work

Also, the superposition of the shear forces gives

$$\begin{bmatrix} Q_x \\ Q_\theta \end{bmatrix} = \begin{bmatrix} V_{\rm st} Q_x^{\rm st} + V_{\rm sh} Q_x^{\rm sh} \\ V_{\rm st} Q_\theta^{\rm st} + V_{\rm sh} Q_\theta^{\rm sh} \end{bmatrix}, \tag{18}$$

where $V_{\rm st}$ and $V_{\rm sh}$ are the volume fractions of the stiffener and the shell, respectively.

3 Cylindrical shell equations

A stiffened composite cylindrical shell, whose schematic view is shown in Fig. 4, is considered here. The governing shell equations in terms of resultant forces and moments including the transverse shear and rotary inertia terms are [33]

$$\begin{aligned} \frac{\partial N_x}{\partial x} + \frac{1}{R}\frac{\partial N_{\theta x}}{\partial \theta} &= I_1 \ddot{u} + I_2 \ddot{\psi}_x, \\ \frac{\partial N_{x\theta}}{\partial x} + \frac{1}{R}\frac{\partial N_\theta}{\partial \theta} + \frac{Q_\theta}{R} &= I_1 \ddot{v} + I_2 \ddot{\psi}_\theta, \\ \frac{\partial Q_x}{\partial x} + \frac{1}{R}\frac{\partial Q_\theta}{\partial \theta} - \frac{N_\theta}{R} - \hat{N}\frac{\partial^2 w}{\partial x^2} + q_n &= I_1 \ddot{w}, \\ \frac{\partial M_x}{\partial x} + \frac{1}{R}\frac{\partial M_{\theta x}}{\partial \theta} - Q_x &= I_2 \ddot{u} + I_3 \ddot{\psi}_x, \\ \frac{\partial M_{x\theta}}{\partial x} + \frac{1}{R}\frac{\partial M_\theta}{\partial \theta} - Q_\theta &= I_2 \ddot{v} + I_3 \ddot{\psi}_\theta, \end{aligned} \tag{19}$$

where I_1, I_2, I_3 are the inertia terms obtained as

$$(I_1, I_2, I_3) = \int_{-\frac{t}{2}}^{\frac{t}{2}} \rho(z)\left(1, z, z^2\right) {\rm d}z. \tag{20}$$

The resultant forces and moments in Eq. (19) are the resultant forces and moments of the shell-stiffener structure and should be substituted from Eqs. (17) and (18).

4 Analytical procedure

Based on the first-order shear deformation theory, the strains and curvatures on the mid-plane surface of the shell can be written as

$$
\begin{aligned}
&\varepsilon^0_{xx} = \frac{\partial u}{\partial x}, \quad \varepsilon^0_{\theta\theta} = \frac{\partial v}{R\partial\theta} + \frac{w}{R},\\
&\varepsilon^0_{x\theta} = \frac{\partial u}{R\partial\theta} + \frac{\partial v}{\partial x}, \quad \varepsilon^0_{\theta z} = \psi_\theta + \frac{\partial w}{R\partial\theta} - \frac{v}{R},\\
&\varepsilon^0_{zx} = \psi_x + \frac{\partial w}{\partial x}, \quad \kappa_x = \frac{\partial \psi_x}{\partial x},\\
&\kappa_x = \frac{\partial \psi_\theta}{R\partial\theta}, \quad \kappa_{x\theta} = \frac{\partial \psi_x}{R\partial\theta} + \frac{\partial \psi_\theta}{\partial x} + \frac{1}{2R}\left(\frac{\partial v}{\partial x} - \frac{\partial u}{R\partial\theta}\right).
\end{aligned}
\tag{21}
$$

Utilizing Eq. (21), Eq. (19) can be expressed in terms of displacement field and its corresponding derivatives as follows:

$$
\begin{aligned}
&A_{11}u_{,xx} + A_{12}\frac{1}{R}(v_{,\theta x} + w_{,x}) + A_{16}\left(\frac{2}{R}u_{,x\theta} + u_{,xx}\right) + A_{26}\frac{1}{R^2}(v_{,\theta\theta} + w_{,\theta}) + A_{66}\frac{1}{R}\left(\frac{u_{,\theta\theta}}{R} + v_{,x\theta}\right)\\
&\quad + B_{11}\psi_{x,xx} + B_{12}\frac{1}{R}\left(\psi_{\theta,\theta x} + \frac{1}{R}v_{,\theta x}\right) + B_{16}\left(\frac{2}{R}\psi_{x,x\theta} + \psi_{\theta,xx} + \frac{v_{,xx}}{R}\right) + B_{26}\frac{1}{R^2}\left(\psi_{\theta,\theta\theta} + \frac{v_{,\theta\theta}}{R}\right)\\
&\quad + B_{66}\frac{1}{R}\left(\frac{\psi_{x,\theta\theta}}{R} + \psi_{\theta,x\theta} + \frac{v_{,x\theta}}{R}\right) = I_1\ddot{u} + I_2\ddot{\psi}_x, \qquad (22a)\\
&A_{12}\frac{1}{R}u_{,x\theta} + A_{22}\frac{1}{R^2}(v_{,\theta\theta} + w_{,\theta}) + A_{16}u_{,xx} + A_{26}\frac{1}{R}\left(\frac{u_{,\theta\theta}}{R} + 2u_{,x\theta}w_{,x}\right) + A_{66}\left(\frac{u_{,x\theta}}{R} + v_{,xx}\right)\\
&\quad + KA_{44}\frac{1}{R}\left(\psi_\theta + \frac{w_{,\theta}}{R} - \frac{v}{R}\right) + KA_{45}\frac{1}{R}(\psi_{,x} + w_{,x}) + B_{12}\frac{1}{R}\psi_{x,x\theta} + B_{22}\frac{1}{R^2}\left(\psi_{\theta,\theta\theta} + \frac{v_{,\theta\theta}}{R}\right)\\
&\quad + B_{16}\psi_{x,xx} + B_{26}\frac{1}{R}\left(\frac{\psi_{x,\theta\theta}}{R} + 2\psi_{\theta,x\theta}\frac{2}{R}v_{,x\theta}\right) + B_{66}\left(\frac{1}{R}\psi_{x,\theta x} + \psi_{\theta,xx} + \frac{1}{R}v_{,xx}\right)\\
&\quad = I_1\ddot{v} + I_2\ddot{\psi}_\theta, \qquad (22b)\\
&-A_{12}\frac{1}{R}u_{,x\theta} - A_{22}\frac{1}{R^2}(v_{,\theta} + w_{)} - A_{26}\frac{1}{R}\left(\frac{u_{,\theta}}{R} + v_{,x}\right) + KA_{44}\frac{1}{R}\left(\psi_{\theta,\theta}\frac{w_{,\theta\theta}}{R} - \frac{v_{,\theta}}{R}\right)\\
&\quad + KA_{45}\left(\psi_{\theta,x} + \frac{w_{,\theta x}}{R} - \frac{v_{,x}}{R} - \frac{w_{,x\theta}}{R} + \frac{\psi_{x,\theta}}{R}\right) + KA_{55}(W_{,xx} + \psi_{x,x}) - B_{12}\frac{1}{R}\psi_{x,x}\\
&\quad - B_{22}\frac{1}{R^2}\left(\psi_{\theta,\theta} + \frac{v_{,\theta}}{R}\right) - B_{26}\frac{1}{R}\left(\psi_{\theta,x} + \frac{\psi_{x,\theta}}{R} + \frac{v_{,x}}{R}\right) = I_1\ddot{w}, \qquad (22c)\\
&-KA_{45}\left(\psi_\theta + \frac{w_{,\theta}}{R} - \frac{v}{R}\right) - KA_{55}(\psi_x + W_{,x}) + B_{11}u_{,xx} + \frac{B_{12}}{R}(u_{,x\theta} + w_{,x}) + B_{16}\left(\frac{2}{R}u_{,x\theta} + v_{,xx}\right)\\
&\quad + \frac{B_{26}}{R^2}(u_{,\theta\theta} + w_{,\theta}) + B_{66}\frac{1}{R}\left(\frac{u_{,\theta\theta}}{R} + U_{,x\theta}\right) + D_{11}\psi_{x,xx} + D_{12}\frac{1}{R}\left(\psi_{\theta,\theta x} + \frac{v_{\theta x}}{R}\right)\\
&\quad + D_{16}\left(\psi_{\theta,xx} + \frac{2}{R}\psi_{x,x\theta} + \frac{V_{,xx}}{R}\right) + D_{26}\frac{1}{R^2}\left(\psi_{\theta,\theta\theta} + \frac{v_{,\theta\theta}}{R}\right) + D_{66}\frac{1}{R}\left(\psi_{\theta,xx} + \frac{\psi_{x,\theta\theta}}{R} + \frac{U_{,x\theta}}{R}\right)\\
&\quad = I_2\ddot{u} + I_3\ddot{\psi}_x, \qquad (22d)\\
&-KA_{44}\left(\psi_\theta + \frac{W_{,\theta}}{R} - \frac{v}{R}\right) - KA_{45}(\psi_x + W_{,x}) + \frac{B_{12}}{R}u_{,x\theta} + \frac{B_{22}}{R^2}(u_{,\theta\theta} + W_{,\theta}) + B_{16}u_{,xx}\\
&\quad + \frac{B_{26}}{R}\left(\frac{u_{,\theta\theta}}{R} + 2v_{,x\theta} + W_{,x}\right) + B_{66}\left(\frac{u_{,x\theta}}{R} + u_{,xx}\right) + \frac{D_{12}}{R}\psi_{x,x\theta} + \frac{D_{22}}{R^2}\left(\psi_{\theta,\theta\theta} + \frac{v_{,\theta\theta}}{R}\right) + D_{16}\psi_{x,xx}\\
&\quad + D_{26}\frac{1}{R}\left(2\psi_{\theta,x\theta} + \frac{\psi_{x,\theta\theta}}{R} + \frac{2}{R}v_{,x\theta}\right) + D_{66}\frac{1}{R}\left(\psi_{x,\theta x} + \psi_{\theta,xx} + \frac{1}{R}v_{,xx}\right) = I_2\ddot{v} + I_3\ddot{\psi}_\theta. \qquad (22e)
\end{aligned}
$$

For a circular cylindrical shell, the displacement field is assumed to be a function of the circumferential wave number n and the axial wave number m. A general expression for the displacement field may be written as

$$
\begin{aligned}
u(x,\theta,t) &= \Psi_u(x)\cos(n\theta)\sin(\omega t),\\
v(x,\theta,t) &= \Psi_v(x)\sin(n\theta)\sin(\omega t),\\
w(x,\theta,t) &= \Psi_w(x)\cos(n\theta)\sin(\omega t),\\
\psi_x(x,\theta,t) &= \Psi_{\psi_x}(x)\cos(n\theta)\sin(\omega t),\\
\psi_\theta(x,\theta,t) &= \Psi_{\psi_\theta}\sin(n\theta)\sin(\omega t),
\end{aligned}
\tag{23}
$$

where ω is the natural frequency of the shell, and Ψ_u, Ψ_v, Ψ_w, Ψ_{ψ_x}, and Ψ_{ψ_θ} are the axial modal functions. The crucial part of the present analysis involves choosing appropriate series forms for these modal functions. A convenient set of Fourier series which satisfies the boundary conditions of a shell with simply-supported ends with no axial constraint (SNA) term-by-term can be given as [16]

$$
\begin{aligned}
\Psi_u(x) &= A_{0n} + \sum_{m=1}^{\infty} A_{mn}\cos\left(\frac{m\pi x}{L}\right),\\
\Psi_v(x) &= \sum_{m=1}^{\infty} B_{mn}\sin\left(\frac{m\pi x}{L}\right),\\
\Psi_w(x) &= \sum_{m=1}^{\infty} C_{mn}\sin\left(\frac{m\pi x}{L}\right),\\
\Psi_{\psi_x}(x) &= D_{0n} + \sum_{m=1}^{\infty} D_{mn}\cos\left(\frac{m\pi x}{L}\right),\\
\Psi_{\psi_\theta}(x) &= \sum_{m=1}^{\infty} E_{mn}\sin\left(\frac{m\pi x}{L}\right).
\end{aligned}
\tag{24}
$$

It is clear that the sine series give zero values at the ends unless one specifies the following affected terms:

$$
\begin{aligned}
\Psi_v(0) &= v_0, \quad & \Psi_v(L) &= v_L,\\
\Psi_w(0) &= w_0, \quad & \Psi_w(L) &= w_L,\\
\Psi_{\psi_\theta}(0) &= \psi_\theta^0, \quad & \Psi_{\psi_\theta}(L) &= \psi_\theta^L.
\end{aligned}
\tag{25}
$$

Substitution of the set of displacement functions and their derivatives into Eqs. (22a)–(22e) leads to an eigenvalue problem whose eigenvalues give the natural frequencies of SNA–SNA stiffened shells. Since the aim is to consider general cases and not necessarily considering any particular type of boundary conditions, a shell with freely supported ends with no tangential constraint (FSNT), which has the end conditions

$$
u = N_{x\theta} = Q_x = \psi_x = M_{x\theta} = 0 \quad (x = 0, L)\,,
\tag{26}
$$

is chosen as a base problem for the set of displacement functions given in Eq. (23). None of the ten boundary conditions given by Eq. (24) are satisfied by the set given in Eq. (24), on a term-by-term basis. Therefore, Stokes' transformation is used to enforce constraints to satisfy the boundary conditions. While differentiating the displacement functions using Stokes' transformation, the end values given by Eq. (25) are required (see the Appendix). The derivative formulas for modal displacement functions are briefly given in the Appendix.

Substituting the set of displacement functions and their derivatives into Eqs. (22a)–(22e), the results can be simplified into two distinct matrix equations in which the Fourier series coefficients are coupled as

$$
\begin{bmatrix}
\lambda_{11} & \lambda_{12} & \lambda_{13} & \lambda_{14} & \lambda_{15}\\
 & \lambda_{22} & \lambda_{23} & \lambda_{24} & \lambda_{25}\\
 & & \lambda_{33} & \lambda_{34} & \lambda_{35}\\
 & Symm. & & \lambda_{44} & \lambda_{45}\\
 & & & & \lambda_{55}
\end{bmatrix}
\begin{bmatrix} A_{mn}\\ B_{mn}\\ C_{mn}\\ D_{mn}\\ E_{mn}\end{bmatrix}
=
\begin{bmatrix} F_1\\ F_2\\ F_3\\ F_4\\ F_5\end{bmatrix}
\tag{27}
$$

and

$$
\begin{bmatrix} \lambda_{01} & \lambda_{02}\\ \lambda_{02} & \lambda_{03}\end{bmatrix}
\begin{bmatrix} A_{0n}\\ D_{0n}\end{bmatrix}
=
\begin{bmatrix} F_6\\ F_7\end{bmatrix},
\tag{28}
$$

where λ_{ij} $(i, j = 1, \ldots, 5)$, λ_{01}, λ_{02}, and λ_{03} are coefficients that depend upon the material properties, the shell frequency, geometrical parameters, and the circumferential and axial wave numbers. The values of F_1 to F_7 are in terms of unspecified end values, N_x^0, N_x^L, M_x^0, M_x^L, v_0, v_L, w_0, w_L, ψ_θ^0, ψ_θ^L, due to applying the Stokes' transformation. Using Eqs. (27) and (28), Fourier coefficients can be expressed explicitly in terms of the ten unspecified boundary quantities. Now, it is necessary to enforce the boundary conditions associated with FSNT shells which are both geometrical and natural types. The geometrical boundary conditions which must be imposed are related to u and ψ_x, while those of natural type are $N_{x\theta} = 0$, $Q_x = 0$, and $M_{x\theta} = 0$ at both ends. For further details, the reader is referred to Refs. [15,16].

This results in a general eigenvalue problem which can be used for any possible combination of boundary conditions. After imposing the constraint conditions due to the geometric and natural boundary conditions, one arrives at the following homogeneous matrix equation:

$$\left[e_{ij}\right]\left[\, N_x^0 \; N_x^L \; M_x^0 \; M_x^L \; v_0 \; v_L \; w_0 \; w_L \; \psi_\theta^0 \; \psi_\theta^L \,\right]^T = [0]\,, \quad (i, j = 1, 2, \ldots, 10). \tag{29}$$

A nontrivial solution for this homogeneous linear system exists if the determinant of the coefficient matrix vanishes. This leads to

$$\left|e_{ij}\right| = 0, \quad (i, j = 1, 2, \ldots, 10), \tag{30}$$

resulting in a characteristic equation whose eigenvalues are the natural frequencies of the FSNT shell. To derive the appropriate characteristic equation of a specified boundary condition, its associated end conditions must be imposed. The characteristic equation required for any type of boundary condition can be extracted by tailoring Eq. (29) in an appropriate way [15]. Therefore, the frequency determinant associated with any specified boundary condition can be derived as a submatrix of the general ten by ten matrix in Eq. (30).

5 Results and discussion

The stiffener cylinder structure (shown in Fig. 4) is considered to be made of Hs-Graphite/epoxy with material properties listed in Table 1. The cylindrical shell is assumed to be four-layered with $[30/-30]_s$ stacking sequence, while in the stiffener structure, fibers are considered to be oriented in the ribs' directions. The geometrical parameters associated with the present model are taken as those reported in Table 2.

Table 3 illustrates a comparison of the natural frequencies obtained via the present analytical approach and those reported by ABAQUS for a SNA–SNA grid-stiffened shell, and good agreement has been achieved. Results are given for four circumferential wave numbers and three different shell thicknesses. As can be seen, the trends of the frequency response obtained from the two analyses agree well. Since ABAQUS considers the structure with its real geometry, it seems that the numerical results given by ABAQUS are closer to the real values of the frequencies. However, from the comparison between the two analyses, it can be concluded that the present analytical scheme is a good as well as capable one for predicting the vibrational behavior of grid-stiffened cylindrical shells. Table 4 gives a comparison between the natural frequencies of stiffened

Table 1 Material properties of Hs-Graphite/epoxy

Hs-Graphite/epoxy		
Young's Modulus (GPa)	E_{11}, E_{22}, E_{33}	181.0, 10.34, 10.34
Shear Modulus (Gpa)	G_{12}, G_{13}, G_{23}	7.2, 7.2, 7.2
Poisson's ratio	$\nu_{12}, \nu_{13}, \nu_{23}$	0.28, 0.28, 0.28
Density (kg/m^3)	ρ	1,389.23

Table 2 Geometrical parameters of the present model

Shell height	254 mm
Shell inner diameter	140 mm
Shell thickness	0.4 mm
Unit cell height	127 mm
Unit cell circumferential length	73.3 mm
Stiffener orientation	$\pm 60^\circ$
Stiffener cross-section	6×6 mm^2

Table 3 Comparison of the natural frequencies reported by two types of analyses for a SNA–SNA stiffened cylindrical shell

n	$t = 0.4$ mm		$t = 0.8$ mm		$t = 1$ mm	
	ABAQUS	Analytic	ABAQUS	Analytic	ABAQUS	Analytic
2	2,057	2,212	2,131	1,908	2,136	1,786
3	1,654	1,421	1,662	1,457	1,663	1,418
4	2,371	2,006	2,445	1,978	2,462	1,959
5	2,947	2,955	3,074	2,817	3,228	2,807

Table 4 Comparison of the natural frequencies for a cylindrical shell with and without stiffeners

n	C–C		SNA–SNA		C–F	
	Unstiffened	Stiffened	Unstiffened	Stiffened	Unstiffened	Stiffened
1	4,781.79	8,852.52	3,704.27	4,675.13	2,456.68	3,924.44
2	2,961.29	5,997.61	1,452.44	2,212.24	1,145.53	1,649.39
3	1,978.48	3,975.93	702.92	1,421.68	638.70	1,239.00
4	1,439.88	3,236.80	542.16	2,006.64	515.47	1,733.64
5	1,192.16	3,532.88	658.09	2,955.40	629.70	2,613.54
6	1,181.91	4,444.06	899.40	4,114.93	867.65	3,732.96
7	1,356.23	5,707.76	1,210.13	5,472.29	1,176.57	5,065.28

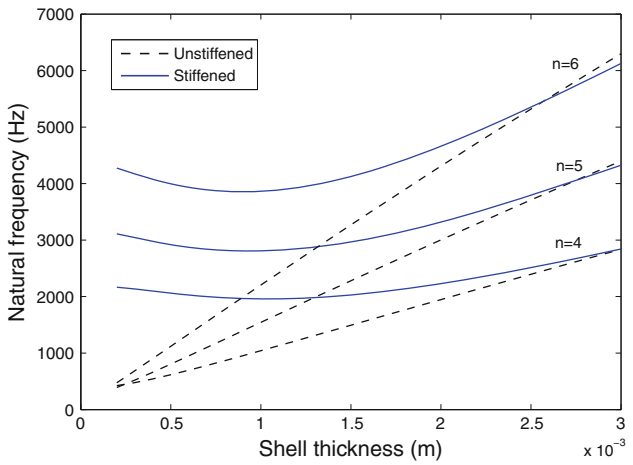

Fig. 5 Variation of the natural frequency with the shell thickness for a SNA–SNA cylindrical shell

and unstiffened cylindrical shells for seven values of circumferential mode numbers and different boundary conditions. The boundary conditions considered here are SNA–SNA, clamped–clamped (C–C), and clamped–free (C–F). As would be observed, the values of the frequencies for the stiffened shell are higher than that of unstiffened shell. This is mainly because of the fact that although the grid structure results into an increase in the mass of the structure, but it increases the stiffness as well and that is why the presence of the grid structure increases the natural frequencies of the shell. As expected before, the fully clamped composite shell has the highest natural frequencies among the selected boundary conditions. In addition, for both stiffened and unstiffened cases, frequency curves converge for circumferential wave numbers greater than six.

Figure 5 exhibits the frequency variation over the shell thickness of a SNA–SNA grid-stiffened cylindrical shell. Results are also compared to those of an unstiffened shell. As can be seen from this figure, the influence of shell thickness variation on the frequency curve is more significant for the unstiffened shell, and the natural frequencies for this case increases by an increment in the shell thickness based upon a nearly linear trend. This is because of the fact that in the case of the unstiffened shell, an increase in the shell thickness increases the stiffness faster than the mass, whereas the trend is different in the case of the grid-stiffened shell. Also, it can be pointed out that for shell thicknesses higher than 2.5 mm, the frequency curves for both stiffened and unstiffened shells converge, and this means that for shell thicknesses greater than a specific value, the presence of the grid structure does not provide any effect on the natural frequency values. Figure 6 depicts the mode shapes of vibration of a grid-stiffened cylindrical shell associated with different boundary conditions.

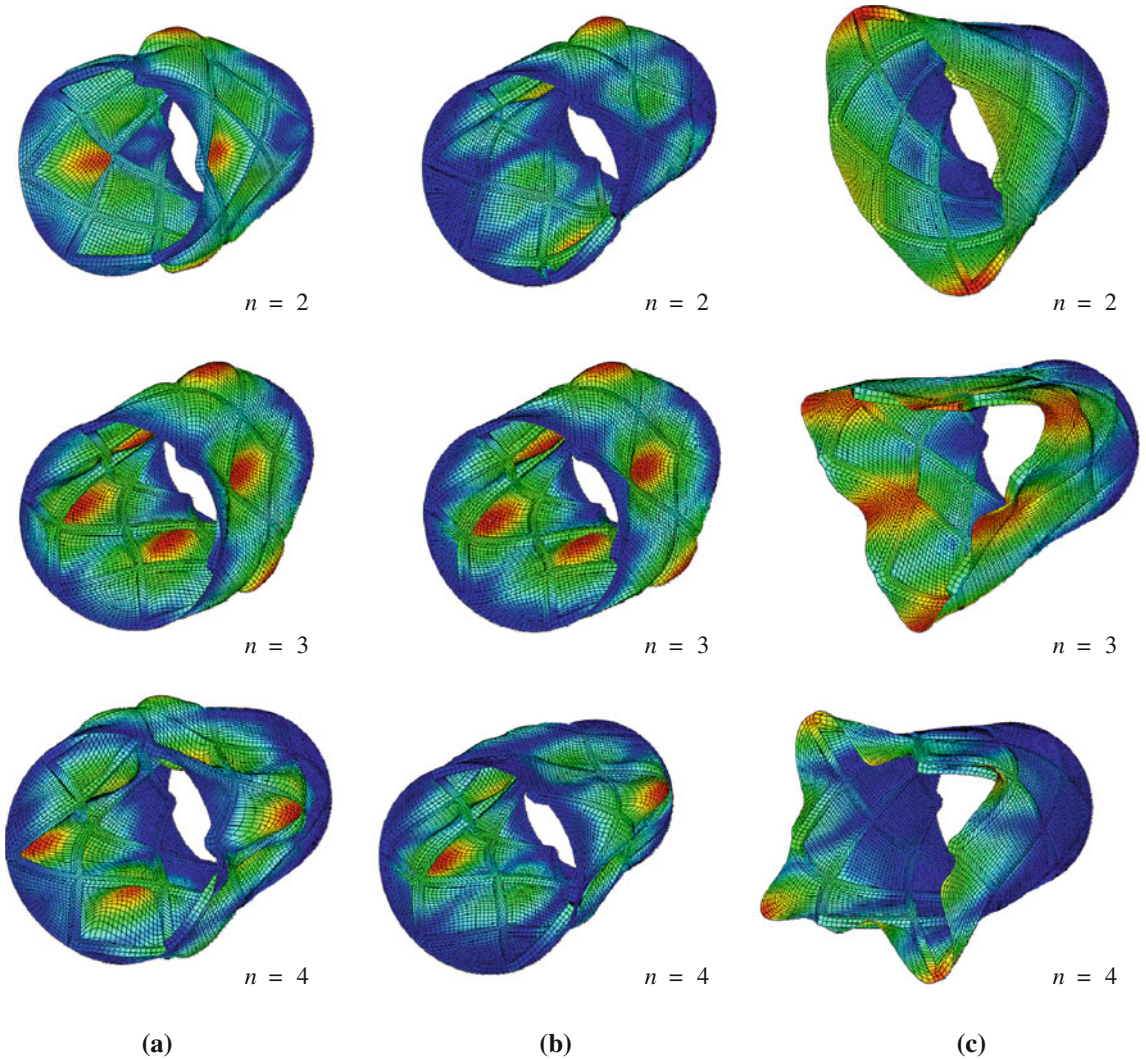

Fig. 6 Mode shapes associated with **a** SNA–SNA, **b** C–C, and **c** C–F grid-stiffened cylindrical shell

6 Conclusions

A unified exact analysis based on Fourier series is employed to investigate the dynamic behavior of grid composite cylindrical shells with cross stiffeners. Theoretical formulations are based on first-order shear deformation shell theory which includes the effects of transverse shear deformation and rotary inertia. A smeared method is employed to superimpose the stiffness contribution of the stiffeners with those of shell in order to obtain the equivalent stiffness parameters of the whole panel. In the smeared method, the flexural behavior of the ribs is also taken into consideration which provides us with a more precise model of the stiffeners. These equivalent stiffnesses will then be entered into the analytical procedure in order to obtain the natural frequencies of vibration. To validate the correctness of the obtained results, a 3-D finite element model is built using the ABAQUS CAE software. The results given are novel and can be used as a benchmark for further studies. The obtained results clarify that the values of the frequencies for the stiffened shell are higher than for the unstiffened shell. This is mainly because of the fact that although the grid structure results in an increase in the mass of the structure, but it increases the stiffness faster and that is why the presence of the grid structure increases the natural frequencies of the shell. Also, the shell thickness has a significant effect on the vibration frequencies of grid shells, and this effect is more pronounced for the unstiffened shell case rather than the stiffened one. Furthermore, for shell thicknesses greater than a specific value, the presence of the grid structure does not provide any effect on the natural frequency values, and the frequency curves associated with both stiffened and unstiffened shells converge.

Appendix: Stokes' transformation

When differentiating a Fourier series, care must be taken with respect to the end values. For example, the end values of the functions represented by sine series are forced to be zero, but using Stokes' transformation, the end values of the sine series are released by being defined separately.

Consider a function $f(x)$ represented by a Fourier sine series in the open range $0 < x < L$ and by values f_0 and f_L at the end points as

$$f(x) = \sum_{n=1}^{\infty} a_n \sin \frac{n\pi x}{L}, \quad 0 < x < L,$$
$$f(0) = f_0, \quad f(L) = f_L,$$

Since we are not sure about the derivative $f'(x)$ to be represented by term-by-term differentiation of the sine series, the derivative is instead represented by an independent cosine series of the following form:

$$f'(x) = b_0 + \sum_{n=1}^{\infty} b_n \cos \frac{n\pi x}{L}.$$

Now, Stokes' transformation consists of integrating by parts in order to obtain the relationship between b_n and a_n as follows:

$$b_n = \frac{2}{L} \int_0^L f'(x) \cos \frac{n\pi x}{L} \mathrm{d}x$$
$$= \frac{2}{L} \left[f(x) \cos \frac{n\pi x}{L} \right]_0^L + \frac{2n\pi}{L^2} \int_0^L f(x) \sin \frac{n\pi x}{L} \mathrm{d}x = \frac{2}{L} \left[(-1)^n f_L - f_0 \right] + \frac{n\pi x}{L} a_n.$$

A similar manner as above must be taken when finding the correct sine series corresponding to $f''(x)$. Therefore, the complete set of derivative formulas for the sine series can be written as

$$\begin{cases} f(x) = \sum_{n=1}^{\infty} a_n \sin \frac{n\pi x}{L}, & 0 < x < L, \\ f(0) = f_0, & f(L) = f_L, \end{cases}$$
$$f'(x) = \frac{f_L - f_0}{L} - \sum_{n=1}^{\infty} \left[\frac{2}{L} \left\{ f_0 - (-1)^n f_L \right\} - \frac{\pi}{L} n a_n \right] \cos \frac{n\pi x}{L}, \quad 0 \le x \le L,$$
$$\begin{cases} f''(x) = \left(\frac{\pi}{L}\right) \sum_{n=1}^{\infty} n \left[\frac{2}{L} \left\{ f_0 - (-1)^n f_L \right\} - \frac{\pi}{L} n a_n \right] \sin \frac{n\pi x}{L}, & 0 < x < L, \\ f''(0) = f_0'', & f(L) = f_L''. \end{cases}$$

Similar transformation formulas must be used to obtain the correct form of the successive derivatives of the cosine series. These formulae are used for the derivatives of displacement functions in the solution procedure of the present analysis. Some of the derivatives of displacement functions are given in the following:

$$u(x, \theta, t) = \left(A_{0n} + \sum_{m=1}^{\infty} A_{mn} \cos \frac{m\pi x}{L} \right) \cos n\theta \sin \omega t, \quad 0 \le x \le L,$$
$$u_{,x} = -\left(\frac{\pi}{L}\right) \sum_{m=1}^{\infty} m A_{mn} \sin \frac{m\pi x}{L} \cos n\theta \sin \omega t, \quad 0 < x < L,$$
$$u_{,x}(0, \theta) = -\left(\frac{\pi^2}{2L}\right) \bar{u}_0 \cos n\theta, \; u_{,x}(L, \theta) = \left(\frac{\pi^2}{2L}\right) \bar{u}_L \cos n\theta,$$
$$u_{,xx} = \left(\frac{\pi}{L}\right)^2 \left[\frac{\bar{u}_0 + \bar{u}_L}{2} + \sum_{m=1}^{\infty} \left\{ \bar{u}_0 + \bar{u}_L (-1)^m - m^2 A_{mn} \right\} \cos \frac{m\pi x}{L} \right] \cos n\theta \sin \omega t, \quad 0 \le x \le L,$$

$$v(x,\theta,t)=\sum_{m=1}^{\infty}B_{mn}\sin(m\pi x/L)\sin n\theta\sin\omega t,\quad 0<x<L,$$

$$v(0,\theta)=-\left(\frac{\pi}{2}\right)v_0\sin n\theta,\ v(L,\theta)=\left(\frac{\pi}{2}\right)v_L\sin n\theta,$$

$$v_{,x}=\left(\frac{\pi}{L}\right)\left[\frac{v_0+v_L}{2}+\sum_{m=1}^{\infty}\left\{v_0+v_L(-1)^m+mB_{mn}\right\}\cos\frac{m\pi x}{L}\right]\sin n\theta\sin\omega t,\quad 0\le x\le L,$$

$$v_{,xx}=-\left(\frac{\pi}{L}\right)^2\left[\sum_{m=1}^{\infty}\left\{v_0m+v_Lm(-1)^m+m^2B_{mn}\right\}\sin\frac{m\pi x}{L}\right]\sin n\theta\sin\omega t,\quad 0<x<L,$$

$$w_{,x}=\left(\frac{\pi}{L}\right)\left[\frac{w_0+w_L}{2}+\sum_{m=1}^{\infty}\left\{w_0+w_L(-1)^m+mC_{mn}\right\}\cos\frac{m\pi x}{L}\right]\cos n\theta\sin\omega t,\quad 0\le x\le L,$$

$$w_{,xx}=-\left(\frac{\pi}{L}\right)^2\left[\sum_{m=1}^{\infty}\left\{w_0m+w_Lm(-1)^m+m^2C_{mn}\right\}\sin\frac{m\pi x}{L}\right]\cos n\theta\sin\omega t,\quad 0<x<L,$$

$$\psi_x(x,\theta,t)=\left(D_{0n}+\sum_{m=1}^{\infty}D_{mn}\cos\left(\frac{m\pi x}{L}\right)\right)\cos(n\theta)\sin(\omega t),\quad 0\le x\le L,$$

$$\psi_{x,x}=-\left(\frac{\pi}{L}\right)\sum_{m=1}^{\infty}mD_{mn}\sin\frac{m\pi x}{L}\cos n\theta\sin\omega t,\quad 0<x<L,$$

$$\psi_{x,x}(0,\theta)=-\left(\frac{\pi^2}{2L}\right)\bar{\psi}_0\cos n\theta,\quad \psi_{x,x}(L,\theta)=\left(\frac{\pi^2}{2L}\right)\bar{\psi}_L\cos n\theta,$$

$$\psi_{x,xx}=\left(\frac{\pi}{L}\right)^2\left[\frac{\bar{\psi}_0+\bar{\psi}_L}{2}+\sum_{m=1}^{\infty}\left\{\bar{\psi}_0+\bar{\psi}_L(-1)^m-m^2D_{mn}\right\}\cos\frac{m\pi x}{L}\right]\cos n\theta\sin\omega t,\quad 0\le x\le L,$$

$$\psi_\theta(x,\theta,t)=\sum_{m=1}^{\infty}E_{mn}\sin(m\pi x/L)\sin n\theta\sin\omega t,\quad 0<x<L,$$

$$\psi_\theta(0,\theta)=-\left(\frac{\pi}{2}\right)\psi_\theta^0\sin n\theta,\ v(L,\theta)=\left(\frac{\pi}{2}\right)\psi_\theta^L\sin n\theta,$$

$$\psi_{\theta_{,x}}=\left(\frac{\pi}{L}\right)\left[\frac{\psi_\theta^0+\psi_\theta^L}{2}+\sum_{m=1}^{\infty}\left\{\psi_\theta^0+\psi_\theta^L(-1)^m+mE_{mn}\right\}\cos\frac{m\pi x}{L}\right]\sin n\theta\sin\omega t,\quad 0\le x\le L,$$

$$\psi_{\theta_{,xx}}=-\left(\frac{\pi}{L}\right)^2\left[\sum_{m=1}^{\infty}\left\{\psi_\theta^0m+\psi_\theta^Lm(-1)^m+m^2E_{mn}\right\}\sin\frac{m\pi x}{L}\right]\sin n\theta\sin\omega t,\quad 0<x<L,$$

The successive derivatives with respect to θ and t are simply achieved. For example, the successive derivatives of $u(x,\theta,t)$ with respect to θ are as follows:

$$u_{,\theta}=-n\left(A_{0n}+\sum_{m=1}^{\infty}A_{mn}\cos\frac{m\pi x}{L}\right)\sin n\theta\sin\omega t,$$

$$u_{,\theta\theta}=-n^2\left(A_{0n}+\sum_{m=1}^{\infty}A_{mn}\cos\frac{m\pi x}{L}\right)\cos n\theta\sin\omega t.$$

References

1. Leissa, A.W.: Vibration of shells, NASA SP-288 US Govt Printing Office (1973)
2. Egle, D.M., Bray, F.M.: An experimental study of free vibration of cylindrical shells with discrete longitudinal stiffening. School of Aero-Space and Mechanical Engineering, University of Oklahoma, NSF Grant, Final Report, GK-1490, November 1968

3. Sharma, C.B.: Calculation of natural frequencies of fixed-free circular cylindrical shells. J. Sound Vib. **35**, 55–76 (1974)
4. Sharma, C.B., Darvizeh, M.: Free vibration characteristics of laminated, orthographic clamped-free cylindrical shells, developments in mechanics. In: Proceedings of the 19th Midwestern Mechanics Conference, Department of Engineering Mechanics, The Ohio State University, Columbus, Ohio, 9–11 September 1985
5. Darvizeh, M.: Free vibration characteristics of orthotropic thin circular cylindrical shell. Ph.D. Dissertation, UMIST (1985)
6. Sharma, C.B., Darvizeh, M., Darvizeh, A.: Free vibration response of multilayered orthotropic fluid-filled circular cylindrical shells. Compos. Struct. **34**, 349–355 (1990)
7. Birman, V.: Exact solution of axisymmetric problems of laminated cylindrical shells with arbitrary boundary conditions: higher-order theory. Mech. Res. Commun. **19**, 219–225 (1992)
8. Lam, K.Y., Loy, C.T.: Influence of boundary conditions and fiber orientation and the natural frequencies of thin orthotropic laminated cylindrical shells. Compos. Struct. **31**, 21–30 (1995)
9. Lam, K.Y., Loy, C.T.: Influence of boundary conditions for a thin laminated rotating cylindrical shell. Compos. Struct. **41**, 215–228 (1998)
10. Darvizeh, M., Haftchenari, H., Darvizeh, A., Ansari, R., Sharma, C.B.: The effect of boundary conditions on the dynamic stability of orthotropic cylinders using a modified exact analysis. Compos. Struct. **74**, 495–502 (2006)
11. Bert, C.W., Malik, M.: Differential quadrature method: a powerful new technique for analysis of composite structures. Compos. Struct. **39**, 179–189 (1997)
12. Sharma, C.B., Darvizeh, M., Darvizeh, A.: Free vibration behavior of helically wound cylindrical shells. Compos. Struct. **44**, 55–62 (1999)
13. Haftchenari, H., Darizeh, M., Darizeh, A., Ansari, R., Sharma, C.B.: Dynamic analysis of composite shells using differential quadrature method (DQM). Compos. Struct. **78**, 292–298 (2007)
14. Ganesan, N., Kadoli, R.: Buckling and dynamic analysis of piezothermoelastic composite cylindrical shell. Compos. Struct. **59**, 45–60 (2003)
15. Kadoli, R., Ganesan, N.: Free vibration and buckling analysis of composite cylindrical shells conveying hot fluid. Compos. Struct. **60**, 19–32 (2003)
16. Ansari, R., Darvizeh, M.: Prediction of dynamic behavior of FGM shells under arbitrary boundary conditions. Compos. Struct. **85**, 284–292 (2008)
17. Hemmatnezhad, M., Ansari, R., Darvizeh, M.: Prediction of vibrational behavior of composite cylindrical shells under various boundary conditions. Appl. Compos. Mater. **17**, 225–241 (2010)
18. Jaunky, N., Knight, N.F., Ambur, D.R.: Optimal design of general stiffened composite circular cylinders for global buckling with strength constraints. Compos. Struct. **41**, 243–252 (1998)
19. Helms, J.E., Li, G., Smith, B.H.: Analysis of grid stiffened cylinders. In: Proceedings of the Engineering Technology Conference on Energy (ASME/ETCE), Houston (2001)
20. Black, S.: A grid stiffened alternative to cored laminates. High Perform. Compos. **10**, 48–51 (2004)
21. Jaunky, N., Knight, N.F., Ambur, D.R.: Formulation of an improved smeared stiffener theory of buckling analysis of grid-stiffened composite panels. NASA technical Memorandum 110162, June 1995
22. Phillips, J.L., Gurdal, Z.: Structural analysis and optimum design of geodesically stiffened composite panels. NASA Report CCMS-90-05, July 1990
23. Gerdon, G., Gurdal, Z.: Optimal design of geodesically stiffened composite cylindrical shells. AIAA J. **23**, 1753–1761 (1985)
24. Jaunky, N., Knight, N.F., Ambur, D.R.: Optimal design of grid stiffened composite panels using global and local buckling analysis. J. Aircraft **35**, 478–486 (1998)
25. Wang, J.T.S., Hsu, T.M.: Discrete analysis of stiffened composite cylindrical shells. AIAA J. **23**, 1753–1761 (1995)
26. Kidane, S., Li, G., Helms, J., Pang, S., Woldesenbet, E.: Buckling load analysis of grid stiffened composite cylinders. Compos. B **34**, 1–9 (2003)
27. Wodesenbet, E., Kidane, S., Pang, S.: Optimization for buckling loads of grid stiffened composite panels. Compos. Struct. **60**, 159–169 (2003)
28. Yazdani, M.: Analytical and experimental buckling analysis of grid stiffened composite shells under axial loading. Ph.D. Dissertation. Tarbiat Modares University, Iran (2009)
29. Yazdani, M., Rahimi, G.H., Afaghi Khatibi, A., Hamzeh, S.: An experimental investigation into the buckling of GFRP stiffened shells under axial loading. Sci. Res. Essay **4**, 914–920 (2009)
30. Yazdani, M., Rahimi, G.H.: The effects of helical ribs' number and grid types on the buckling of thin-walled GFRP-stiffened shells under axial loading. J. Reinf. Plast. Compos. **29**, 2568–2575 (2010)
31. Yazdani, M., Rahimi, G.H.: The behavior of GFRP-stiffened and -unstiffened shells under cyclic axial loading and unloading. J. Reinf. Plast. Compos. **30**, 440–445 (2011)
32. Rahimi, G.H., Zandi, M., Rasouli, S.F.: Analysis of the effect of stiffener profile on buckling strength in composite isogrid stiffened shell under axial loading. Aerosp. Sci. Technol. **24**, 198–203 (2013)
33. Toorani, M.H., Lakis, A.A.: General equations of anisotropic plates and shells including transverse shear deformations, rotary inertia and initial curvature effects. J. Sound Vib. **237**, 561–615 (2000)